Characterization and Modeling of Embroidered NFC Coil Antennas for Wearable Applications

Lulu Xu, Xiao Chen, Sirui Tan, Zhirun Hu, *Member, IEEE*, Baoan Ying, Terry Tao Ye, and Yi Li

***Abstract*—This paper proposes an accurate model for yarn-based embroidered coil antenna used in Near Field Communication (NFC) applications. Traditionally, the inductance of a coil-shaped antenna is calculated using the Wheeler's equation, while accurate enough for metallic coil geometries, the results from Wheeler's equation have more than 20% errors when being applied to yarn-based embroidered antennas. We have discovered that this discrepancy is related to the parasitic capacitance, which is caused by the subtle gaps along twisted fibers. Experiments demonstrate that the parasitic capacitance has significant impact on the overall performances of the coil antenna. In this paper, an equivalent model for yarn-based coils is proposed to take into account of the parasitic capacitance and antenna geometrical characteristics. Compared with traditional Wheeler's equation, the inductance calculated from this proposed model is within 5% from the measured value. Additionally, the electromagnetic performance of the embroidered coil is resilient to mechanical deformation. When being used as a coupling antenna, it can harvest energy and power-up the NFC-based platform for body-area-network applications.**

***Index Terms*—Near field communication (NFC), embroidered electronics, wearable antennas, sensor, e-textiles.**

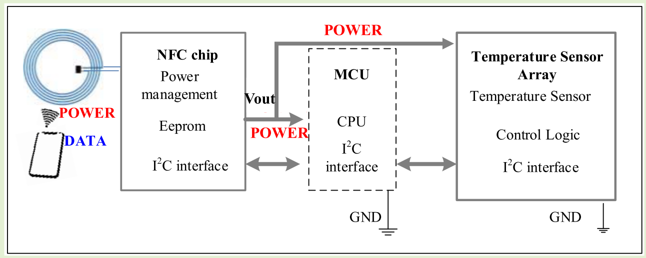

I. Introduction

In recent years, Near Field Communication (NFC) technology has become a promising platform for wireless body area networks (WBAN) applications [1]–[4] and internet of things (IoT) [5]–[8]. With the NFC-enabled mobile phones, the NFC antenna is not only used as a communication channel, it can also be used as a wireless charging source for wearable devices [9], [10]. Wearable NFC antennas with good transmission efficiency and high Q value are of great interest for many wearable applications [11]. For example, Jiang *et al.* reported a wearable NFC system for boy temperature and sweat test, and the device could be integrated into a clothing to realize wireless and unobtrusive monitoring [5].

Typically, the NFC device consists of an inductive coil, a transponder chip, and sometimes, a matching circuitry to tune resonant frequency at 13.56 MHz [12]. The performance of the NFC antenna depends on the inductive coil design [13], [14]. Considerable studies have been focused on the design and modeling of printed PCB or wire bond coil inductors [15]–[18], as well as analysis of transmission efficiency between tags and readers [11], [19], [20]. In NFC design, inductance matching is critical as the well-designed coil can work with a commercial capacitive based NFC chip around 13.56 MHz, and no additional matching circuit is required [21].

For the flexible NFC antenna, its transmission efficiency is relatively poor as compared to the metallic counterparts [2]. This is caused by the high intrinsic resistance of the antenna, which leads to considerable energy loss. For example, the resistance of the circular NFC in [2] was 51 Ω

Manuscript received June 17, 2020; accepted July 6, 2020. Date of publication July 10, 2020; date of current version November 5, 2020. This work was supported in part by the European Union's Horizon 2020 Research and Innovation Program through Marie Skłodowska-Curie under Grant 644268, in part by the University of Manchester through the UMRI Project Graphene-Smart Textiles E-Healthcare Network under Project AA14512, and in part by the British Cotton Growing Abscission: Work People's Collection Fund under Grant R1119938. The associate editor coordinating the review of this article and approving it for publication was Dr. Edward Sazonov. *(Corresponding authors: Terry Tao Ye; Yi Li.)*

Lulu Xu, Sirui Tan, and Yi Li are with the School of Natural Sciences, The University of Manchester, Manchester M13 9PL, U.K. (e-mail: lulu.xu@postgrad.manchester.ac.uk; sirui.tan@postgrad.manchester.ac.uk; henry.yili@manchester.ac.uk).

Xiao Chen is with the Department of Electronic and Electrical Engineering, The University of Sheffield, Sheffield S1 4DE, U.K. (e-mail: xiao.chen@sheffield.ac.uk).

Zhirun Hu is with the School of Electrical and Electronic Engineering, University of Manchester, Manchester M13 9PL, U.K. (e-mail: z.hu@manchester.ac.uk).

Baoan Ying is with the Apparel and Art Design College, Xi'an Polytechnic University, Xi'an 710048, China (e-mail: yingba2006@163.com).

Terry Tao Ye is with the Department of Electrical and Electronic Engineering, Southern University of Science and Technology, Shenzhen 518055, China (e-mail: yet@sustech.edu.cn).

Digital Object Identifier 10.1109/JSEN.2020.3008594

(Q of 9.8); the resistance of the graphene-based NFC in [3] was approximately 33 Ω (Q of 5.0); and the resistance of the printed NFC in [22] was 817 Ω at 13.56 MHz.

Embroidered NFC antennas can directly onto fabrics with conductive yarns have gained more and more attention recently [23]. In 2004, Catrysse *et al.* [24] first embroidered a coil-shaped RFID antenna by stainless steel yarns on a suit. It operated at 700 kHz, collected bi-directional data and harvested energy from incoming radios. Roh [25] investigated inductive characteristics of circular and square inductors. These results suggest that embroidery is a simple and user-friendly process for the fabrication of flexible, lightweight and wearable NFC antennas. While being an attractive approach, compared with traditional metallic coil antennas, many challenges exist for the antenna fabrication, including limited embroidery resolution, high resistivity of conductive yarns and parasitic effects. (Detailed information is shown in Appendix)

An accurate inductive estimation is essential for the design of NFC coil antennas. Harold A. Wheeler's equation for coil-shaped inductance calculations [15] and its modified equations [16] have been widely used for NFC coils design. However, these equations are only valid under restricted conditions, the interval gap between the coil line (s) has to be less than the width of each line (w) ($s < w$), and results are more accurate if the inductance is less than 100 nH. While the embroidered geometries cannot maintain a narrow spacing between lines and the resolution is also very limited. The condition of $s < w$ is hard to achieve, and the accuracy of Wheeler's equations will deteriorate as the ratio s/w increases. In addition, traditional coil model [15] cannot be used to quantify parasitic effects from the yarns, thus the embroidered NFC antenna suffered the deterioration from expected results. To the authors' knowledge, no prior work looked into the limitations of embroidered coils that can be attributed to the microscopic structures of yarns.

In this paper, various circular and square inductive coils with different combinations of geometrical dimensions are embroidered on textile substrates (Section II.A). A new equivalent model is proposed that takes the parasitic capacitance and coil's geometrical characteristics into account. The inductance values derived from this new model are within 5% of the measured results, as compared to over 20% error using traditional Wheeler's equation. (Section II.B, II.C, III.A, III.B and III.C). Through experiments and parameter extraction, the value of parasitic capacitance is estimated (Section III.D and III.E). Based on the accurate modeling, embroidered NFC coil antennas exhibit Q factor from 26 to 41, which are comparable to the metallic ones (Section III.F). When being used on apparels and garments, the embroidered coils can avoid stretching, folding and other deformations (Section III.G). Using the proposed coil as the NFC antenna, it can harvest enough energy to power-up the sensory system (Section IV).

II. Materials and Methods

A. Conductive Yarns and the Embroidery Process

As discussed in Section I, low resistance is preferred for the coil antenna to achieve a high Q factor. Various types of conductive yarns are compared, as shown in Appendix (Table VII). Liberator™ 40 [26] made of silver coated Vectran fibers, with low resistance of 3.3 Ω/m and high tensile strength of 3.0 GPa is selected in this application. Fig. 1 shows SEM images of conductive yarns and embroidered coils. It can be seen that a bundle of metal-clad fibers are twisted and form subtle gaps (g) that increase porosity inside yarns. Equations (1-3) are used to calculate yarns porosity (P), defined as the ratio of the pore area to the yarn area [27].

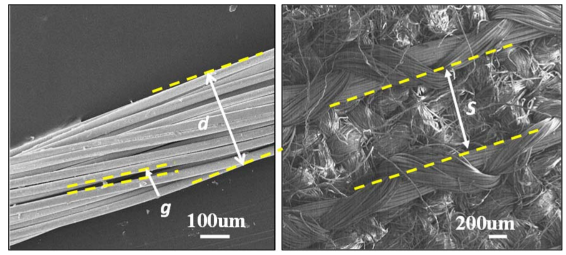

Fig. 1. SEM image of yarn: diameter of the yarns, gaps inside yarns, and line spacing of coil.

$$A_{fiber} = \frac{\text{linear density of yarn}}{\text{Density of fibers}} \tag{1}$$

$$A_{yarn} = \frac{1}{4}\pi d^2 \tag{2}$$

$$P = 1 - \frac{A_{fiber}}{A_{yarn}} \tag{3}$$

where A_{fiber} is the cross-sectional area of fibers, with assumed density of 1.41g/cm^3 [28] and linear density of 0.00126 g/cm. The diameter of Liberator™ 40, $d = 0.04$ cm, as measured from SEM picture. Specifically, we measure the d in Image J software and calculate its value according to the scale of SEM image. The porosity of Liberator™ 40 is about 28.71%, which can induce a considerable parasitic capacitance inside yarns. Details of coils fabrication and embroidery method are shown in Appendix (Fig. 11).

B. Limitations of Traditional Wheeler's Equation

Wheeler's and modified Wheeler's equation for inductance calculation of circular and square coils are in the form of (4) [15], [16]. The geometrical specifications and coefficients (K_1, K_2, K_3) are shown in Fig. 2 and Table I.

$$L_{wheeler} = \frac{K_1 a^2 n^2}{K_2 a + K_3 b} \tag{4}$$

where n is the number of turns of the coil. $a = 0.5(r_i + r_o)$, $b = r_o - r_i$, r_o and r_i are outer radius and inner radius of the coil respectively. $r_i = r_o - n(s + w) - w$.

To parameterize the inductance for yarn-based coil, as well as to test the accuracy of Wheeler's equation, we adopt a semi-empirical 3^3 full factorial experimental scheme (27 samples), in which each sample repeats and tests 3 times. Design of experimental (DOE) samples is shown in Appendix (Table VIII). The impedance values of coils are measured by FieldFox RF Vector Network Analyzer (Keysight AFN9918A-M2).

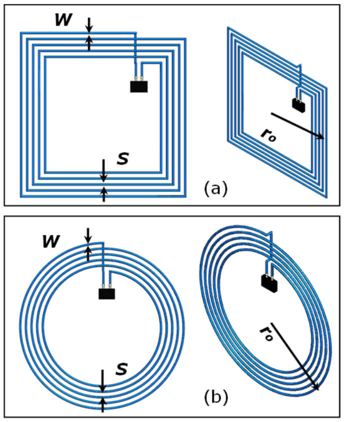

Fig. 2. NFC geometrical specifications. (a) Square shape. (b) Circular shape.

TABLE I
COEFFICIENTS FOR WHEELER'S EXPRESSION

Layout	K_1	K_2	K_3
Circle	3.937×10^{-5}	8	11
Square	1.176×10^{-5}	2	2.75

Fig. 3 illustrates the inductive measurements of conductive yarns-based coils, and comparisons with the calculation from Wheeler's equation. For the horizontal axis of each figure, samples 1-3 are of the same turns of the coil, but their line spacing increases from 0.05 cm, 0.07 cm to 0.09 cm. Similarly tests and parameter combinations are conducted for samples 4-6 and 7-9. As compared to the measurement results, the Wheeler's equations have lower estimation up to 21% and 27% for circular and square coils respectively, and discrepancies increase with the increase of outer radius for both shapes. Thus, Wheeler's equation is no longer a good estimation for the inductance of yarn-based embroidered coil antenna.

C. Equivalent Model of Embroidered Coils

Conventionally, a matching circuit is inserted between the NFC chip and the coil antenna to tuning its operating frequency at 13.56 MHz. In NFC design practice, the antenna is specially tuned to resonate with the equivalent capacitance of the chip, and no matching circuit is needed, as shown in Fig. 4. L_{s-ant} is the intrinsic inductance and can be derived from Wheeler's equation, as:

$$L_{s-ant} = \frac{L_{wheeler}}{\rho_1} \tag{5}$$

ρ_1 is the coefficient of modified inductance for embroidered coil.C_{s-ant} and R_{s-ant} denote its parasitic capacitance and intrinsic resistance respectively. The impedance of the antenna is written as (6):

$$Z_{ant} = \frac{R_{s-ant} + j\omega L_{s-ant}}{1 - \omega^2 L_{s-ant} C_{s-ant} + j\omega R_{s-ant} C_{s-ant}} \tag{6}$$

where ω is the angular frequency with value around 10 MHz, R_{s-ant}, L_{s-ant}, and C_{s-ant}, are of the orders of, 1 Ω, 1 μH, and 1 pF, respectively in NFC applications. With this magnitude of variables in the equation, $|j\omega R_{s-ant} C_{s-ant}| \ll 1|$, the reactant part of (6) can be simplified as (7):

$$I_m\left(Z_{tag}\right) \approx \frac{\omega L_{s-ant}}{1 - \omega^2 L_{s-ant} C_{s-ant}} \tag{7}$$

To realize the reactance-matching between the chip and antenna, we can simplify the reactance part of the impedance Z_{ant} into a single inductance, i.e., the equivalent inductance L_{s-eqv} is expressed in (8). This equivalent inductance already integrates the parasitic capacitance into its value.

$$L_{s-eqv} = \frac{L_{s-ant}}{1 - \omega^2 L_{s-ant} C_{s-ant}} \tag{8}$$

Furthermore, the parasitic capacitance C_{s-ant} is caused by gaps inside the yarns. Quantitatively, C_{s-ant} is proportional to the total length (l_g) of gaps and the thickness (t) of the thread; C_{s-ant} is inversely proportional to the gaps (g) inside of yarns. The parasitic capacitance can be expressed as (9):

$$C_{s-ant} = \frac{l_g t}{g} \varepsilon_{yarn} \tag{9}$$

where ε_{yarn} can be regarded as the absolute permittivity of the combination of air and textile substrate. g and t are values subject to yarns properties. However, due to the intricate subtle gap distributions in the twisted fibers, the exact values of g and t are impossible to quantify.

The length of air gaps along the thread l_g is a geometrical factor, closely related to the length of conductor, and can be calculated based on geometries of the coil, as shown in (10) and (11) for circular and square coils respectively. Variable a has the same definition as that in (4).

$$l_{g-circle} = 2\pi a n \tag{10}$$

$$l_{g-square} = 8an \tag{11}$$

The reciprocal of L_{s-eqv} can be expressed by (12). Substituting (10) or (11) into (9), and further substitute (9) and (5) into (12), the equivalent coil inductance can be expressed in (13).

$$\frac{1}{L_{s-eqv}} = \frac{1 - \omega^2 L_{s-ant} C_{s-ant}}{L_{s-ant}} = \frac{1}{L_{s-ant}} - \omega^2 C_{s-ant} \tag{12}$$

$$L_{s-eqv} = 1/\left(\frac{\rho_1}{L_{wheeler}} - \rho_2 \omega^2 n a\right)$$

$$L_{wheeler} = \frac{K_1 a^2 n^2}{K_2 a + K_3 b} \tag{13}$$

As the variables ε_{yarn}, g and t, are all structure dependent variables and they are hard to quantify with definite values. Here for simplification purpose, we combine these variables into one coefficient ρ_2.

$$\rho_{2-circle} = 2\pi t \varepsilon_{yarn}/g \tag{14}$$

$$\rho_{2-square} = 8t\varepsilon_{yarn}/g \tag{15}$$

The operation resonant frequency is determined by (16) [29], whose accuracy is penalized if neglecting the coil parasitic capacitance C_{s-ant}. The impedance of the NFC chip, along with its reactance-matched antenna impedance, i.e., the

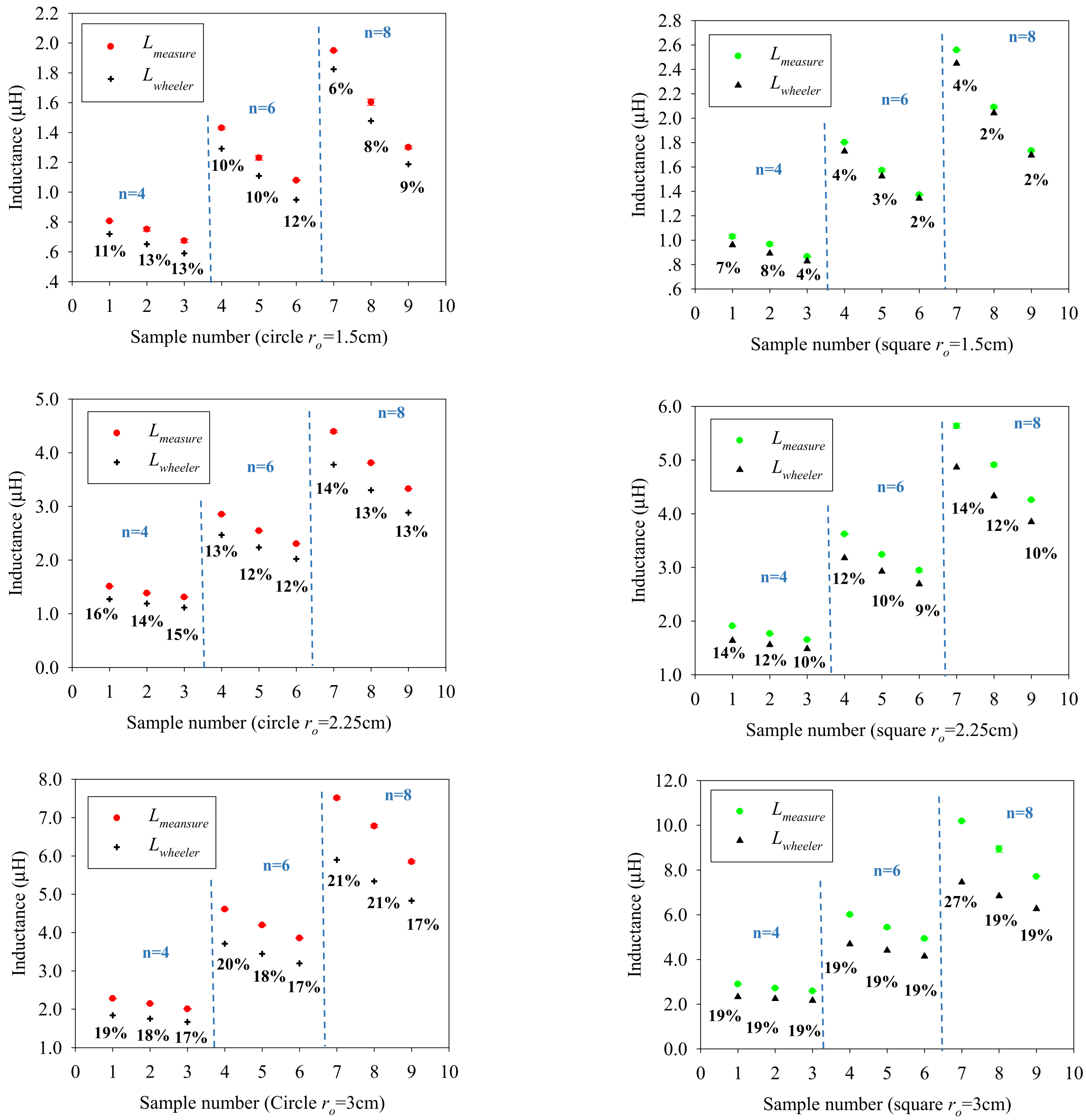

Fig. 3. Measured inductance of circular and square coils.

equivalent inductances, is listed in Appendix (Table IX). When reactance-matched, the NFC antenna and chip can operate at the desired frequency of 13.56 MHz without any tuning circuit.

$$f = \frac{1}{2\pi\sqrt{L_{s-eqv}C_{chip}}} \tag{16}$$

III. Results and Discussion

A. Deriving the Coefficients of the Proposed Model

Based on measured inductance results of 27 samples in II.B and proposed model in Equation (13), we use the curve fitting method (Fig. 12, Appendix) to derive the coefficients (ρ_1 and ρ_2) for circular and square coil respectively. As illustrated in Table II, the measured L_{s-eqv} fits well with the regression model with R-square of 0.997 and 0.994 for circular and square coil respectively.

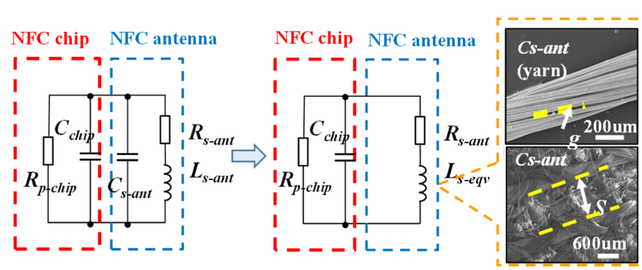

Fig. 4. Equivalent circuit model of the NFC antenna and the NFC chip matching network.

B. Geometrical Parameters and Impacts on Inductance

Factorial design [30] in section II.B not only determines coefficients for L_{s-eqv}, but also address which factor has critical effects on L_{s-eqv}. Minitab (Statistical software release 16)

TABLE II
COEFFICIENT FOR PROPOSED EQUIVALENT INDUCTANCE CALCULATION

Shape	Fit type	ρ_1	$\rho_2\omega^2$	R-square	RMSE
Circular	$z=\rho_1 x-\rho_2\omega^2 y$	0.8828	7.919×10^4	0.997	0.019
Square	$z=\rho_1 x-\rho_2\omega^2 y$	0.9466	1.596×10^5	0.994	0.022

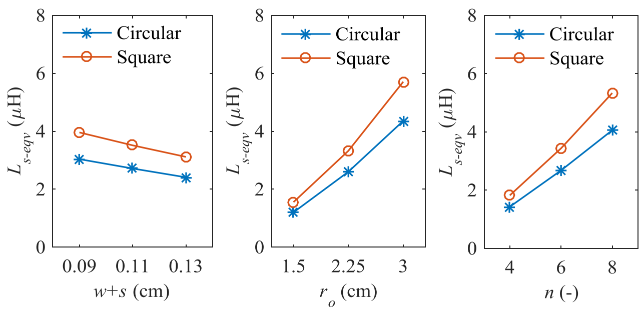

Fig. 5. Geometrical effects of on measured L_{s-eqv}. from Minitab.

is employed in the data analysis of measured inductance. It reveals that the equivalent inductance increases with the increase of the effective area, and vice versa, as shown in Fig. 5. Specifically, it increases when the outer radius and the number of turns increase, and decreases when the line spacing (s) increases. Also, turns and radius show more obvious effects than the line spacing. Therefore, in the NFC coils design, the outer radius and the number of turns are most influential factors for their inductance, while the line width and spacing are secondary factors. The proper line gap between lines can be maintained for NFC coil design to avoid short-circuit and improve fabrication efficiency, while the inductance can be compensated by its outer radius and turn number effectively.

C. Validation of the Equivalent Model

To further validate the accuracy of the inductance calculation of the proposed model, we design and fabricate additional six samples with various geometries for circular and square coils respectively. The parameters are listed in Appendix (Table X) in which the variables belong to proposed model ($1.5 \le r_0 \le 3$ cm, $0.04 \le s \le 0.08$ cm, $4 \le n \le 8$).

By measuring the inductance of these samples, we compare their differences with the proposed model by using Equation (13) and coefficients in Table II. Shown in Fig. 6, the calculated results in proposed model agree reasonably well with the measurement results, within an error of 5%. On the other hand, the results directly from Wheeler's equation create much larger error up to 15%. (Table XII, Appendix).

D. Extraction of the Parasitic Capacitance

The parasitic capacitance is caused by the microstructure of the yarns and its exact value is hard to measure directly. Here we introduce an indirect method to extract the value of the parasitic capacitance, and demonstrate its impact on the overall equivalent inductance.

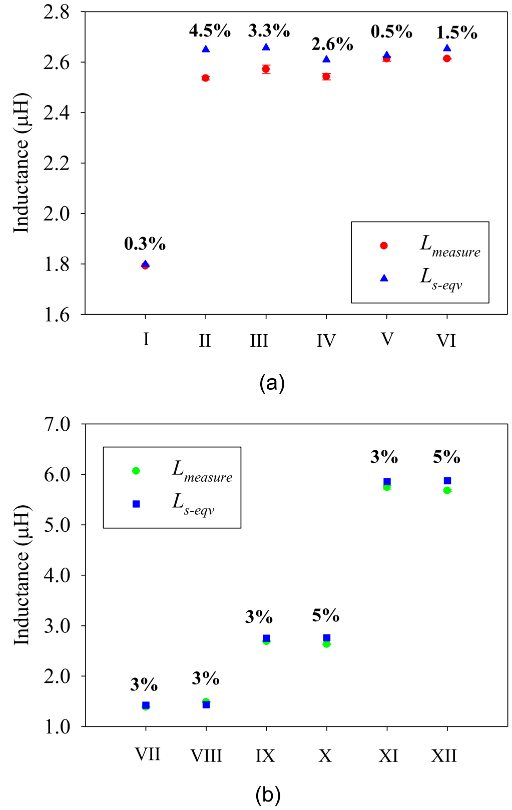

Fig. 6. Measured and calculated inductances of validation samples. (a) Circular coils. (b) Square coils.

From Equation (12) in Section II.C, we can see that at lower frequencies, the parasitic capacitance C_{s-ant} has less impact on the equivalent inductance as compared to higher frequency. In fact, by assuming the operation frequency at 1.0 MHz and plugging corresponding estimation values, we found out that the equivalent inductance L_{s-eqv} is very close to the intrinsic inductance L_{s-ant} of the coil. $L_{s-ant}$and C_{s-ant} will form a self-resonant LC circuit, if we measure the self-resonant frequency, along with the value of L_{s-ant} at 1MHz, noted as L_{1MHz} below. We can derive the parasitic capacitance C_{s-ant} from the following equation:

$$f_0 = 1/(2\pi\sqrt{L_{1MHz}C_{s-ant}}) \tag{17}$$

The measured self-resonant frequencies and measured inductances at 1MHz are listed in Table III, along with the derived parasitic capacitances. It worth noting that, the parasitic capacitance contributes more impacts on equivalent inductance when the coil with larger inductance.

E. Frequency Response of the Embroidery Coils

With the parasitic capacitance, the reactance, or equivalent inductance used in our analysis is no longer constant, and it will change under different frequencies. In fact, the impact of the parasitic capacitance will grow quadratically (with ω^2) as the frequency increases.

Fig. 7 compares the measured equivalent inductance under different frequencies (1-20 MHz) for these twelve samples. It can be seen that the equivalent inductance increases with

TABLE III
MEASURED SELF-RESONANT FREQUENCIES, EQUIVALENT INDUCTANCES AT 1 MHZ AND EXTRACTED PARASITIC CAPACITANCES OF THE VALIDATION SAMPLES

No.	f_0 (MHz)	Measured L_{1MHz} (μH)	$C_{s\text{-}ant}$ (pF)
I	72.5	1.65	2.93
II	58.2	2.42	3.10
III	57.2	2.45	3.16
IV	53.5	2.39	3.70
V	55.4	2.47	3.35
VI	52.0	2.46	3.81
VII	65.6	1.33	4.43
VIII	67.4	1.44	3.88
IX	50.7	2.52	3.91
X	51.2	2.49	3.88
XI	33.7	4.87	4.57
XII	32.8	4.75	4.94

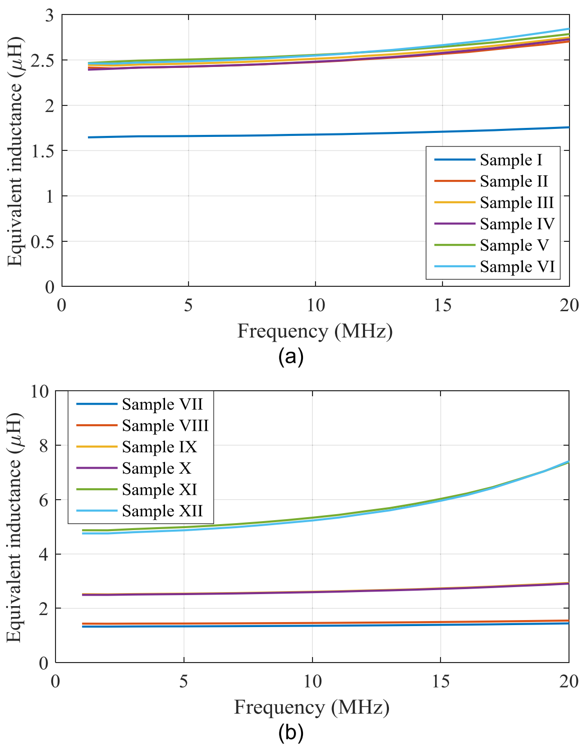

Fig. 7. Measured equivalent inductance variations with frequency. (a) Circular validation samples. (b) Square validation samples.

the increase of frequency for all samples. This phenomenon can be explained with Equation (12), the parasitic capacitance will basically increase the equivalent inductance, and the increase will be more obvious under high frequencies (note the $\omega^2 C_{s-ant}$ part at the denominator of the equation). From Fig. 7, it can also be observed that the increase of the equivalent inductance under high frequency is more significant at higher inductance values. This is because samples with higher inductance have larger size and/or more number of turns, which consequently, result in higher parasitic capacitances (note the C_{s-ant} is proportional to the average radius a and number of turns n as expressed from Equation (8)-(11)).

TABLE IV
CALCULATED EQUIVALENT INDUCTANCES AND MEASURED EQUIVALENT INDUCTANCES AT 13.56 MHZ OF THE VALIDATION SAMPLES

No.	Calculated $L_{13.56MHz}$ (μH)	Measured $L_{13.56MHz}$ (μH)	Error (%)
I	1.71	1.70	0.5%
II	2.56	2.53	0.8%
III	2.59	2.57	0.8%
IV	2.56	2.54	0.5%
V	2.62	2.61	0.3%
VI	2.64	2.62	0.7%
VII	1.39	1.38	0.4%
VIII	1.50	1.48	0.9%
IX	2.71	2.69	0.8%
X	2.68	2.67	0.3%
XI	5.81	5.77	0.7%
XII	4.75	5.69	0.7%

TABLE V
EQUIVALENT INDUCTANCES AT 1 MHZ AND 13.56 MHZ

No.	Measured L_{1MHz} (μH)	Measured $L_{13.56MHz}$ (μH)	Variation (%)	$L_{wheeler}$ (μH)	Error (%)
I	1.65	1.70	3.1%	1.57	-5%
II	2.42	2.53	4.9%	2.29	-5%
III	2.45	2.57	5.2%	2.29	-6%
IV	2.39	2.54	6.3%	2.25	-6%
V	2.47	2.61	6.0%	2.26	-8%
VI	2.46	2.62	6.6%	2.28	-7%
VII	1.33	1.38	4.0%	2.22	-1%
VIII	1.44	1.48	3.3%	2.34	-7%
IX	2.52	2.69	6.8%	2.49	-1%
X	2.49	2.67	7.2%	2.5	0%
XI	4.87	5.77	18.4%	4.8	-1%
XII	4.75	5.69	19.7%	4.81	1%

Substituting the parasitic capacitances derived from Table III into Equation (8), the equivalent inductances at 13.56 MHz can be calculated, as presented in Table IV. It can be seen that the measured inductances agree well with the calculated inductances at 13.56 MHz with errors less than 1%. This validates the introduced parasitic capacitance terms in Equation (8) and (12), and further demonstrates the parasitic capacitance affects the accuracy of equivalent inductance in the proposed model.

We further performed the measurement of the equivalent inductances at 1 MHz and 13.56 MHz, as well as calculated the inductance using Wheeler's equation. Results are listed in Table V. It can be observed that the measured equivalent inductance from 13.56 MHz and 1MHz can have as much as 20% discrepancies. These discrepancies validate that the parasitic capacitances are more obvious under high frequencies. Also listed in the table is the comparison between the measured equivalent inductances at 1 MHz with the calculated results from Wheeler's equation. It can be seen the inductances are slightly underestimated in Wheeler's equation.

F. Q Factor of the Coil

The intrinsic DC resistance of embroidered threads determines the Q factor of the coil antenna. In our design, we have

TABLE VI
LENGTH, DC RESISTANCE, IMPEDANCE AND Q FACTOR OF COILS AT 13.56 MHz

No.	l_g (cm)	DC resistance (Ω)	Impedance (Ω)	Q factor
I	51.24	1.9	3.5+j144.5	41
II	70.59	2.7	5.4+j215.7	40
III	74.11	2.8	5.6+j218.9	39
IV	72.00	2.7	5.6+j216.5	39
V	76.15	2.7	5.2+j222.4	43
VI	79.95	2.8	5.8+j223.3	39
VII	51.60	2.8	4.6+j117.6	26
VIII	54.88	2.3	3.9+j126.3	32
IX	83.04	2.5	6.1+j229	38
X	77.84	2.4	6.0+j227.6	38
XI	128.52	3.5	13.1+j490.9	37
XII	128.96	3.8	14.8+j484.4	33

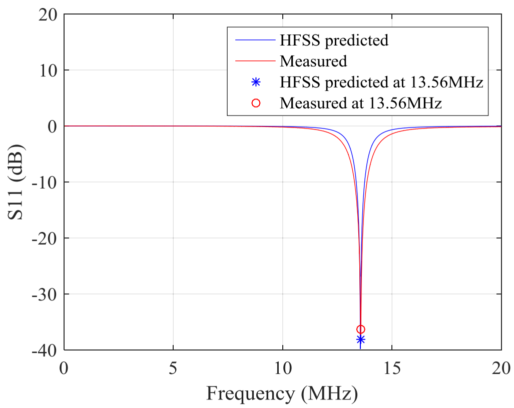

Fig. 8. S11 of conductive yarns-based NFC antenna.

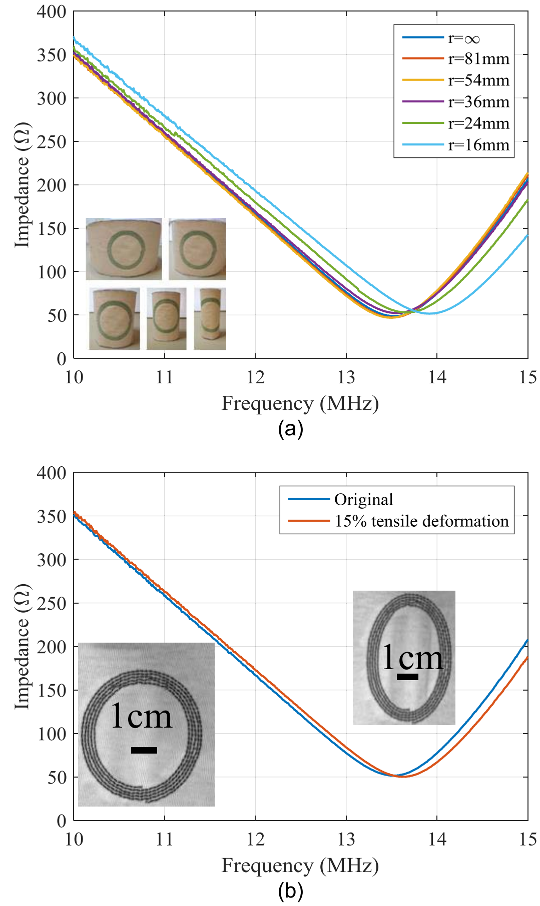

Fig. 9. NFC coil impedance with respect to resonant frequencies under (a) bending and (b) stretching.

employed the process that minimizes the resistance of the embroidered threads. The yarn we selected, Liberator™ 40, has the lowest resistance per unit length compared with other models. The yarn is lightly twisted and its sliver coating could be easily chipped off in high frictional fabrication processes. In order to protect its mechanical and electrical properties, we serve it on bobbin instead of the upper-yarn. In this way, Liberator™ 40 conductivity is well protected to ensure the embroidered NFC antenna to have a low resistance and high Q factor.

The length l_g of the conductive yarns is calculated in Table VI, from which we can see that smaller size coils have lower DC and AC resistances. Q factors are calculated at operating frequency of 13.56 MHz from $Q = 2\pi f_{operating} L_{s-eqv}/R_{AC}$ (Table VI). The embroidered antennas have a high Q factor ranging from 26 to 41, which are higher than what were reported in previous work [25], [31] and are comparable with the commercial coils (Q factors between 10 to 30 [32]).

G. Radiation and Resonant Properties

In order to further test the performance of embroidered coils. We selected the Coil VI and connected it with a resistor and a capacitor. The capacitor value is the same value as the NFC chip capacitance (50 pF) so that the imaginary part of antenna is matched to 0. To minimize the reflected power at resonant point, we use a resistor matched the VNA input impedance (50 Ω) [21]. The experimental measurement of S11 is well consistent with the simulation from ANSYS High Frequency Electromagnetic Field Simulation (HFSS). S11 at 13.56 MHz is approximately −40 dB (Fig. 8), demonstrating the embroidered coil has a good reactance matching with the capacitor.

The antenna consisted of flexible yarn and elastic fabric is naturally soft, flexible and stretchable, which can endure bending, stretching or other deformations from human body [33]. Fig. 9 shows the antenna performance under bending and tensile stretching. Various bending radii (r: 81 mm, 54 mm, 36 mm 24 mm and 16 mm) are designed to represent possible surface curvatures of human body (back, chest, forearm and wrist), as illustrated in Fig. 9(a). It can be observed that the NFC resonant frequency slight increases as the bending curvature increases, i.e., 13.57 MHz at no bending and 14 MHz at the bending curvature of 16 mm. This is because the coil effective area decreases with the bending curvature, which leads to the decrease of inductance and the increase of resonant frequency. Meanwhile, the NFC antenna also shows stable performance under tensile stretching, as shown in Fig. 9(b). It can be seen that the resonant frequency shifts from 13.55MHz (no elongation) to 13.70 MHz (15% elongation).

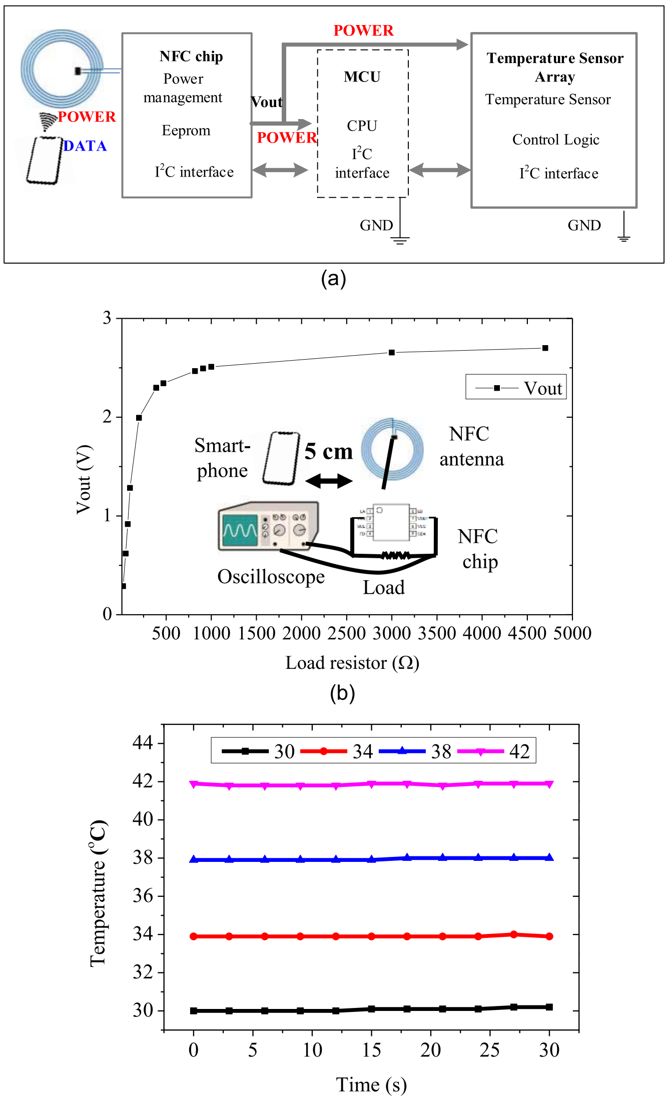

Fig. 10. The energy harvesting performance of embroidered NFC coil. (a) Schematic diagram of the NFC coil driving an MCU chip and a sensor array. (b) Output voltage (driving voltage) from the NTAG chip under different loads. (c) Temperature sensing performance of device under a temperature controlled chamber.

These experiments demonstrate that our designed NFC coil is resilient to deformations. This advantage will benefit its use on WBAN applications.

IV. Application

In NFC systems, the coil that is connected with the NFC chip not only serves as the antenna, it can also harvest the energy coupled from the electromagnetic signal of the reader. We further test the performance of embroidered coil used as the energy harvester. The experiment setup is illustrated in Fig. 10(a). An embroidered coil is connected to the NXP NTAG NFC chip (NT3H2111). The NTAG chip is linked to an MCU chip (MSP430F) through the I2C interface, and then drives a sensor array of 24 temperature sensors (Si7051). NTAG chip provides power supply to its peripheral circuits through the V_{out} terminal, which is the power output from the

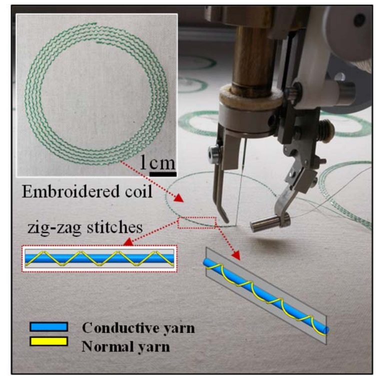

Fig. 11. Image of embroidered coil: conductive yarn warped by the normal yarn with zig-zag stitches.

harvested energy. The MCU and the sensor array are powered up from this terminal. Powered by a smartphone (HUAWEI, P30) with an NFC function from 5 cm away, the embroidered coil can harvest EM energy from the incoming signals. In order to quantify the total harvested energy that can be used to drive the peripherals, we use a variable resistor as the load on the V_{out} pin and increase the resistor from 24 to 4700 Ω, as shown in Fig. 10 (b). The voltage delivered at V_{out} terminal starts from 0.28 V (when the load resistor is 24 Ω) and quickly stabilizes at 2.5 V when the load resistor goes beyond 1000 Ω. From this setup, the NTAG can provide a stable energy of about 6.25 mW with a voltage of 2.5 V. The total estimated power consumption of the MCU, together with 24 temperature sensors, is around 870 μW. Therefore, our proposed embroidered coils can be reliably used as an energy harvester.

This wireless temperature sensing device could be potentially used for breast cancer monitoring. With the temperature array, the temperature profile and the abnormal temperature increase can be detected and sent to the NFC enabled smart phone, then conveyed to back-end servers or cloud, as reported in our separated paper [33]. In order to investigate the wireless temperature sensing performance, we place the device in a chamber with temperature controlled from 30 °C to 42 °C. The temperature of one sensor is recorded by an Android based APP in 30 s interval, as shown in Figure 10(c). It can be seen the reading temperature are steady and match well with the controlled temperature of the chamber. However, from literature [21], we can see the EM energy could be partially adsorbed by human body, which slight reduces the current in the tag. We will focus on human body effects on the NFC antenna and sensors performance in the further.

V. Conclusion

This paper proposed a new circuit model for yarn-based embroidered NFC coil antennas. Because of the porous structure of conductive yarns, parasitic capacitance cannot be neglected in NFC coils design. Traditional coil antenna design uses Wheeler's equation to estimate the inductance, without taking the parasitic capacitance into account. The results from Wheeler's equation have more than 20% discrepancies

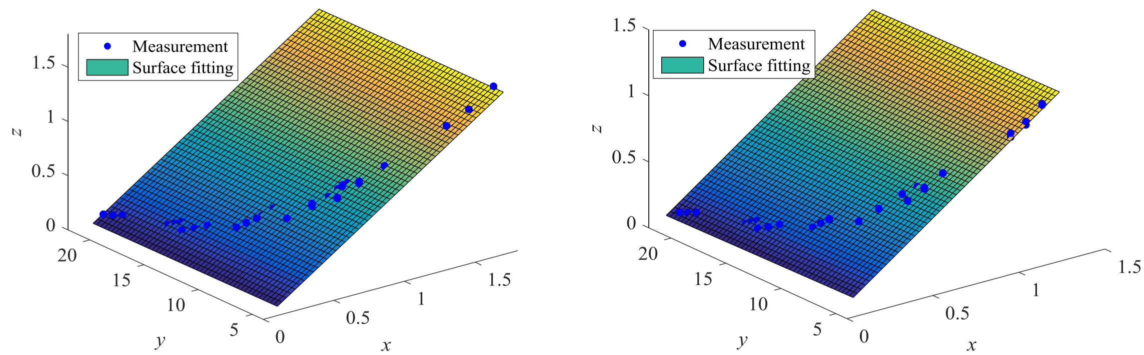

Fig. 12. Surface responses of measured inductance (DOE samples) with fitting functions: x is $1/L_{wheler}$, y is na and z is $1/L_{s-eqv}$. (a) Circular coil. (b) Square coil.

TABLE VII
CHARACTERISTICS OF CONDUCTIVE YARNS [34]

Yarns	Name	DC resistance (Ω/m)	Diameter (mm)	Suppliers	Merits	Demerits
Silver coated	Silverpan 250	50	0.08	TIBTECH Innovations Inc	Lightweight and good elasticity	Break under high tension
Silver plated polyamide yarns	Shieldex® 235/36 dtex 4-ply HC +B	33	0.6	Statex Inc	Anti-static and anti-bacterial	Larger diameter
Nickel-copper braids	Liberator™ 40	3.3	0.4	Syscom Advanced Materials Inc	Lightweight, excellent thermal stability	Light twisted
Stainless steel filament	Thermotech"N"	11	0.7	TIBTECH Innovations Inc	Withstanding sweat, saline water, light oxidation, washable	Heavy-weight; large diameter

from the real values. With our revised model, the equivalent inductance values for both circular and square coils of various sizes are within 5% of measured results. We further extracted the parasitic capacitance of the coil antennas, and correctly demonstrated the frequency response characters of embroidered antennas under different frequencies. Meanwhile, a low-resistance embroidery process is used to minimize the intrinsic resistance of the coils. Using the equivalent model and the optimized embroidering process, the embroidered NFC antenna's S11 parameter is −40 dB at 13.56 MHz, with Q factors ranging from 26 to 41. The embroidered coil also maintains a stable performance under various mechanical deformations. When being used as an antenna in the NFC system, it can provide an ideal battery-free, wireless sensing platform for wearable body networks.

APPENDIX

See Tables VII-XI.

A. Challenges for Embroidery Antennas

1. Embroidering Resolution – Due to the nature of fabrics, the yarn threads cannot maintain geometry with high resolution. Additionally, dangling filaments and broken fibers are unavoidable due to the high friction from the regulator and needle of an embroidery machine. All these factors limit the resolution, as well as the line spacing of the embroidered coils.
2. High Resistivity – Conductive yarns have much higher resistivity as compared to metallic materials. Furthermore, during the embroidering process, conductive yarns will suffer from high tension and moving speed, and result in the breaking and peeling-off of the coating layer or metallic filaments, and further reduce the conductivity of the yarn. For example, in Neil J. Grabham's study [31], coil resistances range from 44 Ω to 120 Ω, much higher than that of copper PCB [35]. It is difficult to achieve high Q factor with this intrinsic resistance of the coil [36].
3. Parasitic Elements – Yarn-based geometries consist of a bundle of fiber filaments twisted tightly. As we will demonstrate in later parts of this paper, subtle gaps will form between/in the threads, which lead to considerable parasitic elements in the equivalent circuit. The antenna properties will deviate from the original calculation if the parasitic effects are not taken into account.

B. Fabrication of the Coil

We use a computer-aided embroidery machine (JCZA 0109-550 (700), ZSK Stickmaschinen GmbH). The machine has two options of embroidery. 1) Conductive yarns with smooth surface can serve as upper yarns, but withstand high stress when yarn crosses through tension generator and needle. 2) Conductive yarns can serve on bobbin fixed by upper normal yarns in a gentle procedure

TABLE VIII
DESIGN OF EXPERIMENT WITH VARIABLES OF THREE LEVELS: RADIUS OF 1.5, 2.25, AND 3 CM; TURNS OF THE COIL OF 4, 6, 8, AND LINE SPACING OF 0.05, 0.07 AND 0.09 CM

No.	s/cm	r_0/cm	n
1	0.05	1.5	4
2	0.07	1.5	4
3	0.09	1.5	4
4	0.05	1.5	6
5	0.07	1.5	6
6	0.09	1.5	6
7	0.05	1.5	8
8	0.07	1.5	8
9	0.09	1.5	8
10	0.05	2.25	4
11	0.07	2.25	4
12	0.09	2.25	4
13	0.05	2.25	6
14	0.07	2.25	6
15	0.09	2.25	6
16	0.05	2.25	8
17	0.07	2.25	8
18	0.09	2.25	8
19	0.05	3	4
20	0.07	3	4
21	0.09	3	4
22	0.05	3	6
23	0.07	3	6
24	0.09	3	6
25	0.05	3	8
26	0.07	3	8
27	0.09	3	8

TABLE IX
THE CAPACITANCE OF COMMERCIAL NFC CHIP, ASSOCIATED WITH DESIRABLE INDUCTANCE TO WORK AT 13.56 MHZ

NFC diode chip	$C_{s\text{-}chip}$ (pF)	$L_{s\text{-}eqv}$ (μH)
ST25TV (ST Microelectronics); ICODE® for smart label such as SL2S2002F, SL2S6002, SL2S2602F, SL2S5302, SL2S5002 (NXP Semiconductor)	23.5	5.86
ST25TA64K (ST Microelectronics)	25	5.12
ST25TV64K (ST Microelectronics)	28.5	4.83
ST25TA (ST Microelectronics) NTAG® SmartSensor, such as NHS31XX; NTAG® for Tags & Labels such as NTAG213/215/216 (NXP Semiconductor);	50	2.75
M24LR04E (ST Microelectronics)	68	2.03
ST25TV (ST Microelectronics) ICODE® for smart label such as SL2S5402, SL2S2102, SL2S5102, SL2S1602 (NXP Semiconductor);	97	1.42

with less tension, protecting the conductive layer of the yarns, and consequently, better conductivity.

Fig. 11 shows the embroidery process, in which the coil is embroidered by placing the conductive yarns on the bobbin, wrapped by normal yarns. The zig-zag stitches are used to fasten the conductive yarn. Liberator™ 40, lighter twisted yarns (Fig. 1), are easily dispersed in high frictional fabrication processes. In Fig. 2, the coil is embroidered by placing the conductive yarns on the bobbin, wrapped by normal yarns. The zig-zag stitches are used to fasten the conductive yarn.

TABLE X
SPECIFICATIONS OF THE VALIDATION SAMPLES

NFC coil	No.	w (cm)	s (cm)	w+s (cm)	r_o (cm)	n
Circular coil	I	0.04	0.05	0.09	1.50	7
	II	0.04	0.07	0.11	2.01	7
	III	0.04	0.09	0.13	2.16	7
	IV	0.04	0.07	0.11	2.26	6
	V	0.04	0.09	0.13	2.43	6
	VI	0.04	0.09	0.13	2.89	5
Square coil	VII	0.04	0.07	0.11	1.59	5
	VIII	0.04	0.05	0.09	1.92	4
	IX	0.04	0.09	0.13	2.14	6
	X	0.04	0.07	0.11	1.80	7
	XI	0.04	0.07	0.11	2.70	7
	XII	0.04	0.09	0.13	2.56	8

TABLE XI
INDUCTIVE CHARACTERISTICS OF VALIDATION SAMPLES

Inductance (μH)	I	II	III	IV	V	VI	VII	VIII	IX	X	XI	XII
$L_{s\text{-}eqv}$	1.80	2.65	2.66	2.61	2.63	2.65	1.42	1.43	2.75	2.76	5.86	5.87
$L_{wheeler}$	1.57	2.29	2.29	2.25	2.26	2.28	1.33	1.33	2.49	2.50	4.80	4.81
1	1.79	2.54	2.56	2.52	2.62	2.61	1.38	1.49	2.69	2.63	5.77	5.66
2	1.79	2.54	2.56	2.52	2.62	2.61	1.38	1.49	2.69	2.63	5.77	5.65
3	1.79	2.54	2.55	2.55	2.63	2.61	1.38	1.49	2.69	2.63	5.77	5.66
4	1.79	2.53	2.57	2.55	2.61	2.61	1.38	1.49	2.68	2.64	5.76	5.69
5	1.79	2.53	2.57	2.56	2.61	2.61	1.38	1.49	2.67	2.64	5.76	5.69
6	1.79	2.53	2.57	2.55	2.60	2.61	1.38	1.49	2.67	2.64	5.77	5.68
7	1.80	2.54	2.59	2.54	2.60	2.61	1.40	1.49	2.70	2.63	5.69	5.68
8	1.79	2.54	2.60	2.55	2.61	2.61	1.40	1.49	2.70	2.63	5.70	5.69
9	1.80	2.54	2.59	2.55	2.61	2.61	1.40	1.49	2.70	2.63	5.70	5.69
Mean of $L_{measure}$	1.79	2.54	2.57	2.54	2.61	2.61	1.38	1.47	2.67	2.63	5.67	5.62
STD of $L_{measure}$	0.3%	0.7%	1.7%	1.3%	1.0%	0.2%	0.8%	0.2%	1.0%	0.5%	3.4%	1.6%
Error of proposed model	0.3%	4.5%	3.3%	2.6%	0.5%	1.5%	2.8%	-2.5%	2.9%	4.9%	3.3%	4.6%
Error of traditional model	-12.4%	-9.9%	-11.0%	-11.5%	-13.5%	-12.7%	-4.1%	-9.1%	-7.1%	-5.0%	-15.2%	-14.4%
Note: 1-9 represent each sample repeats 3 times and tests 3 times.												

For the design of embroidery process, it is important to adjust line width (w) and line spacing (s) to an appropriate trade-off. For an NFC coil, its inductance becomes higher when w/s ratio increases. But due to the resolution limitation, as introduced in Section I, the minimum line spacing should be larger than 0.5 mm to avoid dangling fibers causing short-circuits. As the line gap and line width are closely interrelated, coil designs have to compromise between coil radius and number of turns to ensure the coil have a desirable inductance within limited area.

C. Curve Fitting of the Inductance of NFC Coils

See Fig. 12.

ACKNOWLEDGMENT

The authors would like to thank Ms. Melanie Hoerr, Ms. Britta Sanders and Mr Paul Todd from ZSK, and Dr. Anura Fernando from the University of Manchester for their technical advises in this study.

REFERENCES

[1] B. Zhan, D. Su, S. Liu, and F. Liu, "Wearable near-field communication antennas with magnetic composite films," *AIP Adv.*, vol. 7, no. 6, Jun. 2017, Art. no. 065313.

[2] J. Kim *et al.*, "Battery-free, stretchable optoelectronic systems for wireless optical characterization of the skin," *Sci. Adv.*, vol. 2, no. 8, Aug. 2016, Art. no. e1600418.

[3] A. Scidà *et al.*, "Application of graphene-based flexible antennas in consumer electronic devices," *Mater. Today*, vol. 21, no. 3, pp. 223–230, Apr. 2018.

[4] J. Kim *et al.*, "Miniaturized flexible electronic systems with wireless power and near-field communication capabilities," *Adv. Funct. Mater.*, vol. 25, no. 30, pp. 4761–4767, Aug. 2015.

[5] Y. Jiang, K. Pan, T. Leng, and Z. Hu, "Smart textile integrated wireless powered near field communication (NFC) body temperature and sweat sensing system," *IEEE J. Electromagn., RF Microw. Med. Biol.*, early access, Jul. 22, 2019, doi: 10.1109/JERM.2019.2929676.

[6] A. Abdelgawad and K. Yelamarthi, "Internet of Things (IoT) platform for structure health monitoring," *Wireless Commun. Mobile Comput.*, vol. 2017, pp. 1–10, Jan. 2017.

[7] A. Lazaro, R. Villarino, and D. Girbau, "A survey of NFC sensors based on energy harvesting for IoT applications," *Sensors*, vol. 18, no. 11, p. 3746, Nov. 2018.

[8] P. C. Garrido, G. M. Miraz, I. L. Ruiz, and M. Á. Gómez-Nieto, "A model for the development of NFC context-awareness applications on Internet of Things," in *Proc. 2nd Int. Workshop Near Field Commun.*, Apr. 2010, pp. 9–14.

[9] L. Zhang, Q. Tan, H. Kou, D. Wu, W. Zhang, and J. Xiong, "Highly sensitive NH_3 wireless sensor based on Ag-RGO composite operated at room-temperature," *Sci. Rep.*, vol. 9, no. 1, pp. 1–10, Dec. 2019.

[10] T. Leikanger, J. Häkkinen, and C. Schuss, "Interfacing external sensors with android smartphones through near field communication," *Meas. Sci. Technol.*, vol. 28, no. 4, Apr. 2017, Art. no. 044006.

[11] A. P. Sample, D. A. Meyer, and J. R. Smith, "Analysis, experimental results, and range adaptation of magnetically coupled resonators for wireless power transfer," *IEEE Trans. Ind. Electron.*, vol. 58, no. 2, pp. 544–554, Feb. 2011.

[12] G. Shin *et al.*, "Flexible near-field wireless optoelectronics as subdermal implants for broad applications in optogenetics," *Neuron*, vol. 93, no. 3, pp. 509–521.e3, 2017.

[13] Z. Dibin, N. J. Grabham, L. Clare, B. H. Stark, and S. P. Beeby, "Inductive power transfer in e-textile applications: Reducing the effects of coil misalignment," in *Proc. IEEE Wireless Power Transfer Conf. (WPTC)*, May 2014, pp. 1–4.

[14] X. Chen, F. Lu, and T. T. Ye, "The 'weak spots' in stacked UHF RFID tags in NFC application," in *Proc. IEEE Int. Conf. RFID (IEEE RFID)*, Apr. 2010, pp. 181–186.

[15] H. A. Wheeler, "Simple inductance formulas for radio coils," *Proc. IRE*, vol. 16, no. 10, pp. 1398–1400, Oct. 1928.

[16] S. S. Mohan, M. del Mar Hershenson, S. P. Boyd, and T. H. Lee, "Simple accurate expressions for planar spiral inductances," *IEEE J. Solid-State Circuits*, vol. 34, no. 10, pp. 1419–1424, Oct. 1999.

[17] D.-H. Kim and Y.-J. Park, "Design of a rectangular coil for an effective magnetic resonance wireless power transfer system," in *Proc. IEEE Transp. Electrific. Conf. Expo, Asia–Pacific (ITEC Asia–Pacific)*, Jun. 2016, pp. 680–683.

[18] F. Jolani, Y. Yu, and Z. Chen, "A planar magnetically coupled resonant wireless power transfer system using printed spiral coils," *IEEE Antennas Wireless Propag. Lett.*, vol. 13, pp. 1648–1651, 2014.

[19] O. Jonah, A. Merwaday, S. V. Georgakopoulos, and M. M. Tentzeris, "Spiral resonators for optimally efficient strongly coupled magnetic resonant systems," *Wireless Power Transf.*, vol. 1, no. 1, pp. 21–26, Mar. 2014.

[20] A. K. Ramrakhyani, S. Mirabbasi, and M. Chiao, "Design and optimization of resonance-based efficient wireless power delivery systems for biomedical implants," *IEEE Trans. Biomed. Circuits Syst.*, vol. 5, no. 1, pp. 48–63, Feb. 2011.

[21] Y. Jiang *et al.*, "E-textile embroidered wearable near-field communication RFID antennas," *IET Microw., Antennas Propag.*, vol. 13, no. 1, pp. 99–104, Jan. 2019.

[22] *Standard Test Methods for Stretch Properties of Fabrics Woven From Stretch Yarns*, Standard ASTM D3107-07(2019), 2011.

[23] J.-S. Roh, Y.-S. Chi, and T. J. Kang, "Wearable textile antennas," *Int. J. Fashion Des., Technol. Edu.*, vol. 3, no. 3, pp. 135–153, 2010.

[24] M. Catrysse, R. Puers, C. Hertleer, L. Van Langenhove, H. van Egmond, and D. Matthys, "Towards the integration of textile sensors in a wireless monitoring suit," *Sens. Actuators A, Phys.*, vol. 114, nos. 2–3, pp. 302–311, Sep. 2004.

[25] J.-S. Roh, Y.-S. Chi, J.-H. Lee, S. Nam, and T. J. Kang, "Characterization of embroidered inductors," *Smart Mater. Struct.*, vol. 19, no. 11, Nov. 2010, Art. no. 115020.

[26] Syscom Advanced Materials Ltd. *Liberator 40 Datasheet*. [Online]. Available: http://www.metalcladfibers.com/liberator

[27] S. Chawla, M. Naraghi, and A. Davoudi, "Effect of twist and porosity on the electrical conductivity of carbon nanofiber yarns," *Nanotechnology*, vol. 24, no. 25, Jun. 2013, Art. no. 255708.

[28] Marlow Roples Ltd. *Material Properties*. [Online]. Available: https://www.marlowropes.com/material-properties

[29] C. A. Balanis, *Antenna Theory: Analysis and Design*, 4th ed. Hoboken, NJ, USA: Wiley, 2016.

[30] D. Montgomery, *Design and Analysis of Experiments*, 5th ed. New York, NY, USA: Wiley, 2001.

[31] N. J. Grabham, Y. Li, L. R. Clare, B. H. Stark, and S. P. Beeby, "Fabrication techniques for manufacturing flexible coils on textiles for inductive power transfer," *IEEE Sensors J.*, vol. 18, no. 6, pp. 2599–2606, Mar. 2018.

[32] J. Kim *et al.*, "Epidermal electronics with advanced capabilities in near-field communication," *Small*, vol. 11, no. 8, pp. 906–912, Feb. 2015.

[33] L. Xu *et al.*, "Deformation-resilient embroidered near field communication antenna and energy harvesters for wearable applications," *Adv. Intell. Syst.*, vol. 1, no. 6, Oct. 2019, Art. no. 1900056.

[34] L. Xu, Y. Liu, Y. Li, P. Y. Lau, H. Si, and T. T. Ye, "Design and fabrication of embroidered RFID antennas for wearable applications," in *Proc. IEEE Int. Conf. Service Oper. Logistics, Inf. (SOLI)*, Jul./Aug. 2018, pp. 118–122.

[35] A. Tsolis, W. Whittow, A. Alexandridis, and J. Vardaxoglou, "Embroidery and related manufacturing techniques for wearable antennas: Challenges and opportunities," *Electronics*, vol. 3, no. 2, pp. 314–338, May 2014.

[36] L. L. Xu, Y. Li, Y. T. Jang, Z. R. Hu, Y. X. Shi, and W. Xu, "A review on wearable NFC antenna devices," in *Proc. Textile Bioeng. Informat. Symp.*, vol. 1, Y. Li and W. L. Xu, Eds. Hong Kong: Textile Bioengineering Informatics Society Ltd, 2017, pp. 131–145.

Lulu Xu was born in 1990. She is currently pursuing the Ph.D. degree in textile science and technology with the Department of Materials, The University of Manchester. Her research interests include wearable sensors, e-textiles, and wireless communication.

Xiao Chen received the B.Eng. and M.Sc. degrees in electrical engineering from the Harbin Institute of Technology, China, in 2009 and 2011, respectively, and the Ph.D. degree in electrical machines from the University of Sheffield, U.K., in 2015. He is a Lecturer with the Electrical Machines and Drives Group, Department of Electrical and Electronics Engineering, University of Sheffield. His current research interests include manufacturing-led innovation in electrical machines, multi-phase fault tolerant electrical machines for more electric aircraft, digital twin of electrical machine and drive, high-speed electrical machines for traction, low-cost electrical machines, and powertrain energy management for electric vehicles.

Sirui Tan is currently pursuing the Ph.D. degree in textile science and technology with the Department of Materials, The University of Manchester. His research interests include embroidery sensors, graphene coated electrodes, and actuator.

Zhirun Hu (Member, IEEE) received the B.Eng. degree in telecommunication engineering from the Nanjing University of Posts and Telecommunications, Nanjing, China, in 1982, the master's degree in business administration, and the Ph.D. degree in electrical and electronic engineering from the Queen's University of Belfast, U.K., in 1988 and 1991, respectively. He is a Professor with the Department of Electrical and Electronics Engineering, The University of Manchester. He has published more than 200 peer reviewed journal articles and conference papers. His current research interests include in Graphene/2D materials RF electronics, wearable electronics, RF/microwave/millimeter-wave device, circuit and antenna modeling, optimization, design, realization, and characterization.

Baoan Ying received the B.Sc. degree in mechanical manufacturing technology and automatic from the Huazhong University of Science and Technology, China, in 1984, the M.Sc. degree in computer integrated manufacturing system from the North-West Institute of Textile Science, China, in 1990, and the Ph.D. degree in functional textile and clothing from Hong Kong Polytechnic University, China, in 2005. He is an Associate Professor with the Clothing and Art Design College, Xi'an Polytechnic University, China. His current research interests include computer-aided design, computer graphics, numerical simulation, functional textile and clothing, product development, and knowledge management.

Terry Tao Ye received the Bachelor of Science degree in electronic engineering from Tsinghua University, Beijing, in 1993, and the Ph.D. degree in electrical engineering from Stanford University in 2003. He is a Professor with the Department of Electrical and Electronics Engineering, Southern University of Science and Technology (SUSTech). Beside his academic activities, he is also keen on industry-academic collaborations. He had held various engineering and consulting roles in China Academy of Science, Impinj Inc, Synopsys Inc., Magma Design Automation Inc., Silicon Architects Inc., and many other Silicon Valley companies.

Yi Li is a Full Professor and the Chair of Textile Science and Engineering with the School of Natural Sciences, The University of Manchester. He is a Life Fellow of the Royal Society of Art, Commerce, and Manufacturing and International Biographical Association and a Fellow of the Textile Institute, and an Adjunct Professor of a number of universities in China and a member of several professional bodies. He has supervised over 50 Ph.D. students and more than 140 research personnel. He has over 500 scientific publications, including 433 SCI/CPCI articles and peer-reviewed conference papers with 10603 citations and h-index of 55 and i10-index 207 as being recognized as an international leading expert in smart functional textiles. He is selected on the list of Highly Cited Researcher in 2013 by Thomson Reuters. He is the Chairman of Textile Bioengineering and Informatics Society and the Editor-in-Chief of the *Journal of Fiber Bioengineering and Informatics*.